Millimeter-Wave Measurements of Foliage Attenuation and Ground Reflectivity of Tree Stands at Nadir Incidence

Adib Y. Nashashibi, *Senior Member, IEEE*, Kama Sarabandi, *Fellow, IEEE*, Shadi Oveisgharan, M. Craig Dobson, *Senior Member, IEEE*, Wayne S. Walker, and E. Burke, *Senior Member, IEEE*

***Abstract*—In this paper, the phenomenology of wave propagation through foliage and forest ground reflectivity is investigated for assessing the feasibility of foliage-covered target detection at millimeter-wave frequencies. An experimental procedure for simultaneous measurements of foliage attenuation and ground reflectivity is outlined. This measurement procedure is implemented for two different tree stands, one mostly coniferous and the other deciduous, using a nadir-looking, high-resolution, 35-GHz radar positioned above the tree canopy. Statistics of the two-way attenuation and ground reflectivity for these two well-characterized stands are derived. Strong spatial and angular fluctuations in the two-way foliage attenuation coefficient are observed. The mean, standard deviation, and median of the measured two-way attenuation factor at Stand 1 (mostly coniferous trees with 0.140 trees/m^2 stocking density and 45.45 Kg/m^2 green biomass) are -25.4, -18.3, and -48.2 dB, respectively, while the mean, standard deviation, and median of the measured two-way attenuation factor at Stand 2 (deciduous trees with 0.1055 trees/m^2 stocking density and 30.90 Kg/m^2 green biomass) are -15.4, -12.7, and -33.6 dB, respectively. The mean attenuation rates of Stand 1 and Stand 2, derived from the measured two-way attenuation factor, are 0.40 and 0.24 Np/m, respectively. Only a small percentage of the data had two-way foliage attenuation values exceeding 70 dB. The mean, standard deviation, and median of the power reflectivity of the forest floor at Stand 1 are -14.2, -11.0, and -21.1 dB, respectively, while for Stand 2, the same statistical measures are -16.0, -14.3, and -22.2 dB, respectively. The results demonstrate the potential for using MMW nadir-looking radars for the detection of targets underneath foliage-cover.**

***Index Terms*—Attentuation measurement, millimeter wave propagation, millimeter wave radar, radar detection.**

I. Introduction

DETECTION and identification of targets in a strong clutter background, such as a target over a rough terrain, or embedded in a random medium, such as a target camouflaged under a forest canopy, have long been a subject of intensive investigation. Whereas significant progress have been made toward the development of detection and identification algorithms of targets over a clutter background, through the application of multisensor systems such as optical, thermal, lidar, and radar systems, the detection of foliage-covered targets with the required probability of detection and false alarm rate remains at large an unsolved problem. The main goal of foliage-concealed target detection is to develop means to electromagnetically interrogate a composite scene of target plus vegetation in such a manner as to either: 1) penetrate the canopy without corrupting the phase and amplitude of the return from the target of interest, or 2) use the return from the canopy itself to establish the distortion matrix for the effects of the clutter and subsequently account for these effects in order to electromagnetically "defoliate" the scene. Due to exorbitant attenuation of electromagnetic waves at optical and infrared frequencies, the application of conventional optical and IR sensors for detecting a target hidden under foliage has been proven to be unsatisfactory. However, due to the ability of electromagnetic waves to penetrate through foliage, particularly at low microwave frequencies, the application of ultra-wideband imaging radars for detection and identification of targets positioned under foliage have been investigated [1]–[5] primarily in a side-looking configuration. So far, the thrust of investigation on foliage penetrating radars has been focused on the frequency range covering HF through UHF band. Both boom-based [2], [5] ultra-wideband SAR radars (spanning the frequency range between 50 and 1200 MHz) and airborne [3], [4] multifrequency (VHF, UHF, *L*, and *C*-bands) SAR radars were used to examine the attenuation and backscatter statistics of forested areas and in hard target detection studies. The rationale behind this choice of frequency range is an intuitive one, basically, the lower is the radar frequency, the lower is the attenuation and scattering from branches and tree trunks. However, there are two drawbacks in this approach that have somewhat limited the success of low-frequency foliage penetrating radars: The first is the relatively low resolution of these systems due to the limited available bandwidth and the second is the low radar cross section of some targets of interest at these frequencies which are comparable to the scattering from tree trunk and ground interaction or large branches.

Having recognized the aforementioned challenges and difficulties associated with the existing foliage penetrating side-looking radars, we have reexamined the problem and considered millimeter-wave (MMW) nadir-looking radars for this application. The premise for this research stems from the fact that electromagnetic signals at millimeter-wave (MMW)

Manuscript received May 16, 2002; revised June 30, 2003. This work was supported by the Defense Advanced Research Projects Agency (DARPA) through the Army Research Office under Contracts DAAD 19-00-1-0115 and DAAD 19-02-10262.

A. Y. Nashashibi, K. Sarabandi, S. Oveisgharan, M. C. Dobson, and W. S. Walker are with the Department of Electrical Engineering and Computer Science, The University of Michigan, Ann Arbor, MI 48109-2122 USA (e-mail nuha@umic.edu).

E. Burke is with the The Army Research Laboratory, Adelphi, Maryland 20783 USA.

Digital Object Identifier 10.1109/TAP.2004.827250

frequencies can penetrate through few layers of foliage with some finite attenuation and the fact that there is a considerable number of openings through most foliage covers. Furthermore, very high resolution and far more compact radar systems can be designed at millimeter-wave frequencies, hence, they can be operated successfully in a nadir-looking configuration. The nadir-looking configuration has two main advantages over the side-looking configuration: The first is that the total two-way foliage attenuation is expected to be minimal for a nadir-looking radar since the ray path length is minimal at normal incidence and the second is the dependence of the attenuation rate on the incidence angle. A tree trunk is the largest scatterer in a tree structure that can produce significant shadowing, especially, for observation points in its near-field region [6]. However, at near normal incidence, vertical tree trunks do not contribute significantly to either attenuation or scattering. It sould be pointed out that nadir-looking MMW radars are not expected to replace side-looking low-frequency radars. The side-looking low-frequency radar has the primary benefit of being a standoff system, enabling wide-area coverage, while the nadir-looking MMW radar can be used for relatively narrow-area coverage and to confirm the presence of targets in areas initially flagged by the low-frequency radar.

To evaluate the performance of the nadir-looking MMW radar system, phenomenology issues pertaining to electromagnetic wave interaction with foliage at MMW frequencies must be studied. Of particular interest are the attenuation and phase defect of a wave propagating through, and to a lesser extent scattering from vegetation. Attenuation is important for path-loss calculations which is in turn needed for estimating the required transmitter power and for signal-to-noise calculations. Phase defect refers to the fluctuation of radar backscatter from a point target on the forest floor as a function of the aspect angle. This phase fluctuation is directly related to the angular decorrelation function of the backscattered return from the forest media. A synthetic aperture radar (SAR) forms a radar image with high resolution in azimuth by observing a scatterer over a relatively narrow range of aspect angles. Basically by correcting the two-way phase history of the backscatter signal (assuming free-space propagation) from a stationary target, the radar beam can be focused on the target. Any deviation in the signal phase from that of the free-space propagation will degrade the azimuthal resolution of the radar. Direct scattering from foliage is also important as the target backscatter has to compete with that of the foliage which fall within the same range-bin. Hence, the phenomenology study of wave propagation in foliage at MMW frequencies becomes an essential step toward the development of an optimal target detection algorithm. Such a study involves the characterization of signal attenuation and phase defect as a function of both electrical and physical parameters of foliage constituents, such as relative permittivity, density, size, and orientation distributions of leaves, branches, and needles. In addition to foliage attenuation and phase defect, the reflectivity of the forest ground at nadir incidence will have a significant impact on both the system design and on the detection algorithm and needs to be examined as well. A number of research efforts aimed at characterizing experimentally the propagation and bistatic scattering of MMW signals in tree canopies have been reported previously [7]–[14]. However, the experimental results reported in the literature are acquired entirely at near-grazing incidence. In addition, both measurements and semi-empirical models of the MMW radar backscattered return from bare soil surfaces have been reported at both low and high incidence angles [15], [16], none however of actual forest grounds at nadir incidence.

In this paper, outdoor experimental procedures as well as two-way foliage attenuation and ground reflectivity data acquired using a nadir-looking radar operating at 35-GHz are presented. Phase defect is not considered in this investigation and will be the subject of a separate paper. The outdoor measurements were conducted in the State of Maryland, on two distinct well-characterized tree stands one being mostly coniferous (henceforth referred to as Stand 1) and the other deciduous (henceforth referred to as Stand 2). The foliage parameters of these stands, including tree density, height, trunk diameter, location, foliage coverage, etc., were also characterized accurately and summarized in this paper.

II. Outdoor Measurement Technique

Traditionally, attenuation measurements are conducted using two disjoint antennas, one operating as a transmitter and the other operating as a receiver. The system is setup such that the two antennas are operated in a line-of-sight measurement mode with the random medium (in this case the foliage) positioned between the two antennas. There are three main difficulties associated with this technique: 1) a complicated experimental setup is required, in which both the transmitting and receiving antennas need to maintain their relative positions and orientations as they scan the canopy; 2) amplitude and phase fluctuations between the transmitter and the receiver must be minimized at all times while long microwave cables carrying the reference signal move with the antennas inside the canopy; and 3) a complicated calibration procedure is needed to keep track of the orientations of the antennas with respect to the surface.

Due to the inherent difficulties in the line-of-sight measurement technique, we have deployed a monostatic radar above the tree canopy and positioned a calibration target with known radar cross section (such as a corner reflector) underneath the canopy along the radar antenna boresight. Statistics of field attenuation were obtained by moving both the radar and the target to different spots. The purpose of the point target is to reflect the radar signal that has penetrated the foliage layer back toward the radar. On the down-side, the two-way attenuation measurements require a far more sensitive receiver. However, this configuration overcomes the difficulties associated with the two-antenna technique while imitating what a radar signal endures during the target detection measurements.

The experimental setup used in performing the outdoor attenuation measurements is depicted in Fig. 1. In this setup, a trihedral is used as the reference target under the tree canopy. The trihedral is positioned atop a Styrofoam pedestal above the ground. The height above the ground for the corner reflector is selected such that the return from the trihedral could be isolated from that of the ground surface in time domain. The radar used in this experiment operates in a frequency chirped-pulse mode with a bandwidth of 500-MHz capable of producing a 30-cm range resolution.

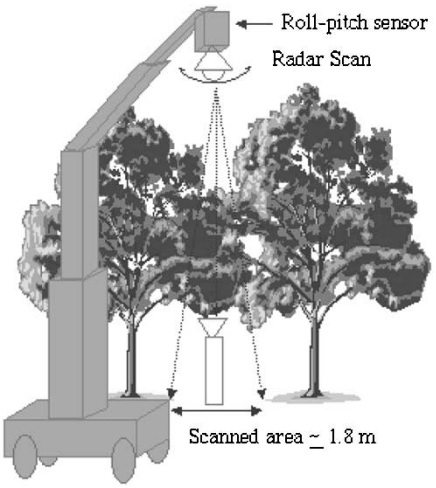

Fig. 1. Outdoor experimental setup used during the attenuation measurements.

According to the radar equation, the return power from a trihedral with radar cross-section (RCS) σ_t, in free-space, can be computed from

$$P_{rt}^f = \frac{\lambda^2 G_t G_r \sigma_t}{(4\pi)^3 R_t^4} P_t = K \frac{\sigma_t}{R_t^4} P_t \tag{1}$$

where

$$K = G_t G_r \frac{\lambda^2}{(4\pi)^3}. \tag{2}$$

P_{rt}^f and P_t are the received and transmitted powers, respectively, λ is the radar wavelength, G_t and G_r are the transmit and receive antenna gains, respectively, and R_t is the range to the trihedral. This equation can easily be modified to account for the effect of foliage assuming that the incident phase-front illuminating the trihedral is uniform. This condition is satisfied, if the trihedral is relatively far from the nearby scatterers. In the presence of foliage, the received power is a random variable whose statistics are influenced by the physical parameters of the foliage cover. The average received power $\bar{P}_r$ can be related to an average two-way foliage attenuation factor A. Using (1), the average received power from a trihedral measured in backscatter under a statistically uniform canopy can be obtained from

$$\bar{P}_{rt}^c = \frac{K}{R_t^4} \sigma_t A P_t. \tag{3}$$

Maintaining the radar configuration (range, transmitter power, etc.) the same, A can simply be obtained from

$$A = \frac{\bar{P}_{rt}^c}{P_{rt}^f} \tag{4}$$

where P_{rt}^f is measured by placing a trihedral outside the test stand (in the absence of any foliage cover). Fluctuations in the radar receiver gain and transmitter power over the duration of the experiment was monitored by observing a leakage between the transmitter and receiver. The effect of system fluctuations was removed from the measured data used in the computation of P_{rt}^c.

A. Ground Reflectivity Measurements

Also of great importance is the forest floor reflectivity measurements. Due to radar size, far-field criterion, and mobility limitations, the radar system usually cannot be deployed under the canopy crown for ground reflectivity measurements. However, the data collected from the trihedrals can be used to estimate the average ground reflectivity from the backscatter measurements. To demonstrate the procedure let us consider a radar system above a ground plane in a nadir-looking configuration. If the ground-air interface is smooth and the radar is far from the interface, image theory can be invoked and the received power can be calculated from *Friis* transmission formula. Representing the distance between the radar and ground by R_g, the received power can be computed by

$$P_{rg}^f = \frac{\lambda^2 G_t G_r}{(4\pi)^2 (2R_g)^2} P_t \Gamma \tag{5}$$

where Γ is the power reflectivity at normal incidence. For a smooth dielectric interface $\Gamma = |\rho_f|^2$, where ρ_f is the Fresnel reflection coefficient.

The forest floor is usually rough and covered with vegetation litter which scatter the incident energy in directions other than backscatter. Therefore, the forest ground reflectivity may be significantly smaller than the Fresnel power reflectivity. The statistics of the measured backscatter power from the ground is influenced by the canopy and surface roughness as well as the density and distribution of vegetation litter on the ground. However these two processes are mutually independent and one can easily show that

$$\bar{P}_{rg}^c = \pi K \frac{P_t}{R_g^2} A \bar{\Gamma} \tag{6}$$

where $\bar{\Gamma}$ is the average ground reflectivity of the forest floor. Taking the ratio of (3) and (6), P_t can be eliminated and $\bar{\Gamma}$ can be obtained from

$$\bar{\Gamma} = \frac{\sigma_t R_g^2}{\pi R_t^4} \frac{\bar{P}_{rg}^c}{\bar{P}_{rt}^c} \tag{7}$$

Expression (7) can be used directly if the experiment is conducted with and without the trihedrals assuming that the radar remains calibrated throughout both experiments. However, if the shadowing effect of the trihedral can be accounted for, one experiment would be sufficient to measure both the two-way attenuation and ground reflectivity. Beside circumventing an additional set of measurements, the single-measurement approach does not require system calibration. In this approach the time-domain responses are examined individually from which P_{rg}^c, P_{rt}^c, and the corresponding ranges to the radar are extracted as shown in Fig. 2.

To account for the shadowing effect of the trihedral on the measured ground reflectivity, the following observations are in order. The physical dimensions of the calibration trihedral are much larger than a wavelength and therefore physical optics approximation can be used to evaluate its bistatic scattering cross section. Physical optics approximation provides very accurate results along directions which correspond to a stationary-phase point of the radiation integral and the forward

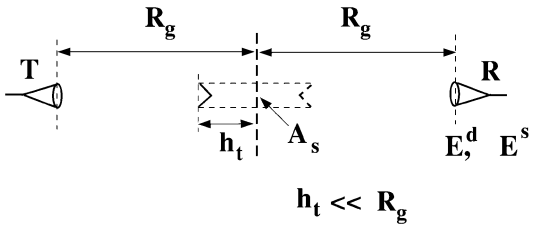

Fig. 2. Geometry of a trihedral positioned along the boresight between a transmitter and a receiver. E^d is the direct field from the transmitter in the absence of the trihedral. E^s is the scattered field from the trihedral (and its image) at the receiver.

scattering direction [18]. According to physical optics approximation the amplitude of the forward scattered field is directly proportional to the area intercepted by the incident wave (the area of the object's shadow (A_s) on a plane perpendicular to the direction of incident wave) and is given by [19]

$$S = \frac{iA_s}{\lambda}. \tag{8}$$

Fig. 2 shows the geometry of the forward scattering problem which is obtained by applying the image theory. Since the height of the trihedral above the ground is relatively small (compared to the radar range to the trihedral) the forward scattering of the trihedral and its image is the same as that of the trihedral alone. Basically the shadow area of the composite target is approximately the same as that of the trihedral alone. Noting that the path lengths for the direct wave to the receiver (E^d) and the scattered wave from the trihedral to the receiver (E^s) are the same, after some simple algebraic manipulations, the *Friis* transmission formula can be modified as follows:

$$\frac{P_{rg}^c}{P_t} = \frac{G_r G_t \lambda^2}{(4\pi R_g)^2}\left|\frac{1}{2} + \frac{S}{R_g}\right|^2 \cdot \bar{\Gamma} \cdot A \tag{9}$$

Equation (9) reduces to the *Friis* transmission formula when $S = 0$. It should also be noted that the phase of S is near 180° which results in a reduction in P_{rg}^c. Basically $|(1/2) + (S/R_g)|^2 \leq 1/4$. It is also obvious that as the range to the target/ground is increased, the effect of point target shadowing diminishes. In view of (9), (7) can be modified and the ground reflectivity in the presence of a trihedral can be obtained from

$$\bar{\Gamma} = \frac{\sigma_t R_g^2}{4\pi R_t^4 \left|\frac{1}{2} + \frac{S}{R_g}\right|^2} \frac{P_{rg}^c}{P_{rt}^c} \tag{10}$$

where P_{rg}^c and P_{rt}^c can be directly obtained from the time-domain radar backscatter measurements.

III. Experimental Setup and Measurement Procedure

A heavy-duty, self-propelled crane, owned and operated by Army Research Laboratory (ARL) personnel, was used to lift the radar system and position it above the tree canopy (about 24–26 m above ground). The crane was driven on a paved road at the edge of the tree stands. As depicted in Fig. 1, the crane consisted of a four-wheeled main chassis and a two-section boom. The lower section was fully extended to ensure a minimum radar height of about 24 m while the upper section was tilted such that it was parallel to the ground surface. With the nadir-looking radar system suspended at the tip of the upper section, it was possible to position the radar above any preselected spot on the ground by moving the crane on the road and by extending or retracting the upper section of the boom. A fully polarimetric Ka-Band radar operating at a center frequency of 35-GHz and effective beamwidth of 2° was deployed. The radar employs a fast frequency chirp modulation of 500 MHz bandwidth [17] (30-cm range resolution).

As mentioned before, characterization of the average two-way foliage attenuation cannot be accomplished with just a single measurement of a trihedral under the canopy. To capture the variability of foliage cover within a given tree stand, multiple measurements are required at many locations. To perform these measurements accurately, the trihedral had to be moved manually from one spot to the next according to a well-characterized grid on the ground. The grid consisted of 30 to 32 rows (depending on the tree stand) with 10 spots in each row. The spots were about 1 meter apart and the rows were perpendicular to the road where the crane was parked. A subset of these rows were selected for the foliage attenuation measurements to ensure that foliage cover be present over the entire row. We also excluded spots that were too close to tree trunks. A 12-inch trihedral having an RCS of $\sigma_t = 21$ dBsm was mounted atop a Styrofoam pedestal 90 cm above the ground. As expected, a difference of 6 ns was observed between the times of arrival of the radar returns from the trihedral and ground beneath it.

To determine the exact location on the ground where the trihedral is to be positioned within a given row, a 10-m-long rope was stretched near the ground directly below and parallel to the boom. The photograph in Fig. 3 shows the rope deployed at Stand 1 (mostly coniferous) along with the trihedral facing upward atop the Styrofoam pedestal. The rope was marked at increments of 1 meter. To ensure that the rope was directly below the upper section of the boom and parallel to it, an alignment technique was used. Once the radar system was ready for measurements, the boom was first raised to the proper height above the road where the crane was located. With the upper section of the boom fully retracted, the trihedral was positioned under the radar system (on the Styrofoam pedestal) and moved in azimuth until a maximum radar return from the trihedral was observed. Then, the distance from the trihedral to the boom truck frame was measured. This distance is the same offset distance needed between the frame and the first point in the transect (i.e., the first marking on the rope). The position of the trihedral was confirmed using a low-power laser that was attached to the 35-GHz radar and aligned parallel to the radar beam. During the attenuation measurements, the laser spot was observed on the ground near the trihedral in areas with low foliage cover. These observations confirmed that both the incremental extension of the upper section of the boom and positioning of the trihedral at a given spot were performed correctly. It should also be noted that the 2° beamwidth of the 35-GHz radar resulted in an effective footprint of about one meter in diameter (at a range of 26 m). Hence, small errors (<15 cm) in positioning the trihedral were tolerated since they would not affect the attenuation measurements significantly.

Fig. 3. Photographic picture showing the transect (yellow rope) and the trihedral facing upward atop a Styrofoam pedestal.

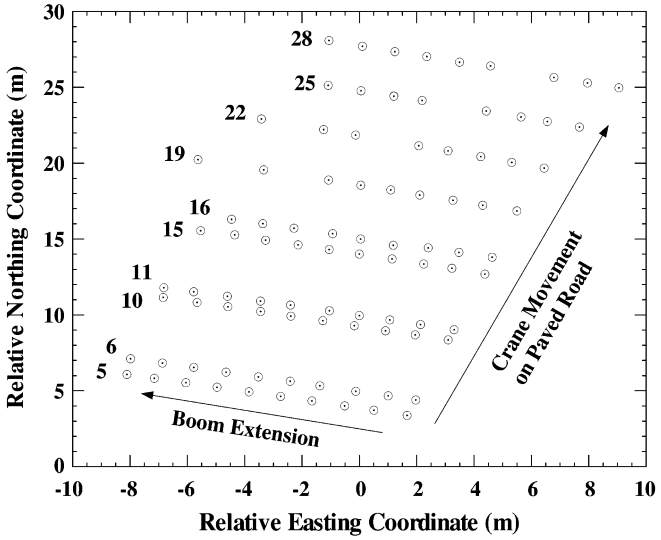

Fig. 4. Relative GPS coordinates of the spots that were measured at Stand 1. These coordinates were computed relative to the coordinates of a point located at the edge of the tree stand.

The radar system was mounted on a gimbal at the tip of the boom giving it the ability to mechanically scan its antenna beam in a plane perpendicular to the upper section of the boom. This feature was used during the attenuation measurements to scan around nadir incidence (0°). At each spot, data was collected at three incidence angles $-1°, 0°$, and $+1°$. The radar scan was performed to reduce the probability of the radar foot-print missing the trihedral. A 1° change in the incidence angle, corresponded to a 0.45-m shift in radar's foot-print on the ground (when the radar was positioned 26 m above the ground). In addition, multiple measurements were performed at each incidence angle and at any given spot. For each incidence angle, 16 and 8 measurements were performed at Stands 1 and 2, respectively. The time lapse between these successive measurements was three seconds. In effect, the radar dwelled on the trihedral for about 48 and 24 seconds at Stands 1 and 2, respectively. The rational behind these long dwell times was to take advantage of the wind induced temporal variations that often occurs in the locations and orientations of the foliage constituents. These temporal variations permit the generation of statistically independent realizations of the foliage layer, hence, a better estimate of the mean two-way attenuation over that particular spot. It should be noted that in most cases, the strongest mean radar return of the trihedral was detected at 0° incidence, as expected, and the data from the other angles were ignored. The foliage cover condition for each spot, the wind condition, and signal-to-noise ratio of the trihedral return, were recorded during the experiments. At Stand 1, 10 rows were selected for measurements. Indices for these rows were 5, 6, 10, 11, 15, 16, 19, 22, 25, and 28. Ten spots were selected in each row and the radar measurements were performed over three incidence angles $(-1°, 0°, +1°)$. At Stand 2, the selected rows were 11, 18, 26, and 31. In this Stand, the measurements were performed slightly differently where instead of positioning the trihedral at a single spot directly below the radar system, the trihedral was positioned at three different spots: directly below the radar, one meter to the left, and one meter to the right of the rope. With this approach more measurements could be performed for a given row. For each of the three trihedral positions, the radar was oriented such that its main antenna beam coincided with the position of the trihedral. In effect, the attenuation measurements were performed at the following sets of incidence angles: $(-3°, -2°, -1°), (-1°, 0°, +1°)$, and $(1°, 2°, 3°)$.

A differential GPS method was used to acquire an accurate 3-D position of the radar above the canopy. The GPS rover unit was incorporated into the radar system at the end of the boom. The rover unit was connected through a wireless spread spectrum communication module to the stationary GPS unit, a base-station, located at a nearby surveyed spot of known coordinates. Running the differential mode, the GPS rover was able to determine its relative position in longitude, latitude, and height with an accuracy of 1 to 2 cm. The GPS antenna for the rover unit was attached to the boom directly above the radar system. During measurements, the rover unit was queried by the data acquisition code and the received GPS data, along with the radar data, were incorporated into a single output file. The GPS data was used in the signal processing stage to correct for errors in the radar height due to boom sagging. The GPS coordinates of the spots that were measured at Stand 1 are shown in Fig. 4. These coordinates were computed relative to a point at the edge of the stand for convenience. In addition to the GPS system, a roll-pitch (RP) sensor with $0.1°$ accuracy was mounted on top of the radar system frame in order to monitor the radar's orientation. Boom sagging not only results in an error in the radar height but also in an error in the radar look angle which translates to an offset in the location of the radar foot print on the ground. The RP sensor was used in a real-time mode to determine the radar's orientation and correct for errors in the radar look-angle due to sagging in the upper section of the boom.

A. Physical Characterization of the Tree Stands

In order to make the measured results useful, the physical parameters of the two test stands, such as number density of trees, average tree height, biomass, etc., must be well-characterized. The adopted ground sampling protocols were consistent with Unites States Forest Service (USFS) National Forest Inventory and Analysis (FIA) inventory program. For each stand, a rectangular plot encompassing the area to be observed was established

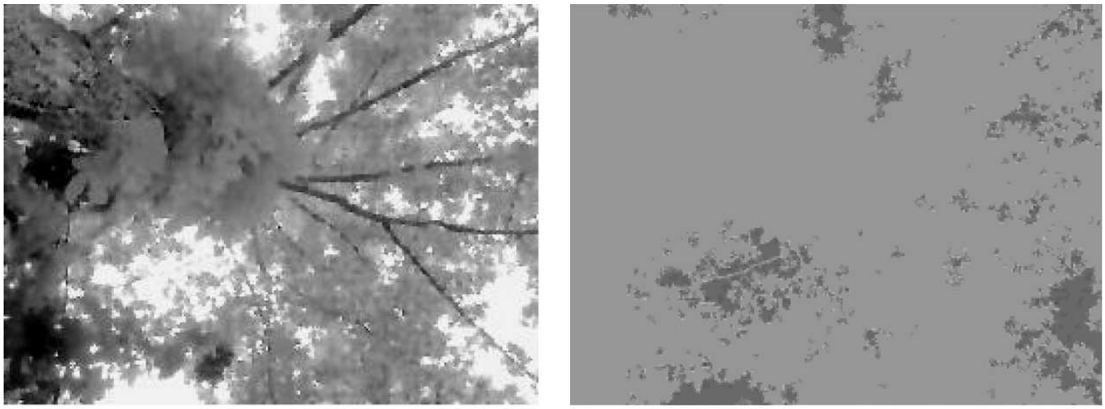

(a) (b)

Fig. 5. An example of (a) an original digital photograph taken at Stand 2 from ground level of the canopy and (b) the image after classification.

using a compass, laser finder, and fiberglass tapes. For all woody stems >5 cm in diameter at breast height (DBH), the species, stem number, and diameter were recorded. The 3-D structure for each stem was then characterized by measuring the total tree height, the height of the live crown, and the crown diameter. In addition, the *x-y* location to the nearest meter was measured for each stem. Each stem was assigned a crown shape class, classified as being either live or dead, and classified as having either a dominant/codominant or nondominant canopy positions. Leaf-area-index (leaf area/ground surface area m^2/m^3) for each stand was determined from measurements using an LI-COR 2000 Plant canopy Analyzer at both ground level and above ground-cover.

For tree Stand 1 (mostly coniferous), the site is dominated by a plantation of mature Loblolly pine (Pinus tiada) over topping a significant understory/small overstory hardwood component. The pine stand appears to have been thinned in the recent past allowing for the proliferation of hardwoods including Sweetgum (Liquidambar styraciflua), Yellow poplar (Liriodendron tulipifera), and Black cherry (Prunus serotina). Trees (>5 cm DBH) measured within the test area averaged 17.8 cm in diameter (standard deviation (std) of 11.8 cm) and 13.1 m in height (std of 6.6 m). Height to live crown (i.e., live canopy) averaged 5.8 m (std of 4.6 m) whereas total crown thickness averaged 7.3 m (std of 4.0 m). Stocking density and basal area values were relatively high, averaging 0.140 trees/m^2 and 0.00444 m^2/m^2, respectively. Understory shrubs were uncommon and ground cover was largely absent due to the presence of a thick pine litter layer. The average leaf area index and ground cover thickness at Stand 1 were 4.23 m^2/m^3 (std of 0.56 m^2/m^3) and 73.4 cm (std of 59.1 cm), respectively.

For tree Stand 2 (deciduous), the site is characterized by an even-aged stand of Sweetgum with a highly disturbed understory/ground-cover layer of vines (poison ivy), briars (rose and raspberry), and invasive shrubs (autumn olive). Trees (>5 cm DBH) measured within the experimental area averaged 18.0 cm in diameter (std of 9 cm) and 11.5 m in height (std of 5.4 m). Height to live crown (i.e., live canopy) averaged just 4.1 m (std of 2.2 m) whereas total crown thickness averaged 7.4 m (std of 4.5 m). Stocking density and basal area exhibited moderate to high values, averaging 0.1055 trees/m^2 and 0.00324 m^2/m^2, respectively. The stand is relatively open and the tree canopies are relatively thin, i.e., considerable light penetration occurs. Shrub cover in the understory/ground-cover layer is dense to the point that traversing the area is difficult. The leaf area index and ground cover thickness at Stand 2 were 4.33 m^2/m^3 (std of 0.76 m^2/m^3) and 43.4 cm (std of 17.9 cm), respectively. The LAI at this stand is unexpectedly high, indicating a possible error in LI-COR measurements.

Percentage open sky (seen upward from the forest floor) was also determined at both stands. The percentage open sky for a canopy is defined as the fraction of open sky to the total observed area in a prescribed solid angle for a given direction. It was determined as follows: High resolution digital photographs (1.23 million pixels in each photograph) were taken straight up at various places within the test site. An unsupervised per-pixel image classification procedure was then used to assign each color into a class. These classes were then manually interpreted and reduced to two classes only: sky, not-sky. A photograph of the foliage-cover taken from a point on the ground at Stand 2 showing sky openings is shown in Fig. 5(a) as an example. Fig. 5(b) shows the same picture where the sky openings and foliage are classified into two groups. At the end of classification process, the number of sky pixels were calculated as well as the fraction of total pixels. The average percentage open sky at Stand 1 and Stand 2 were 9.54% and 24.23%, respectively.

Comparisons between the stocking density, basal area, volume, and green biomass of Stand 1 (mostly coniferous) and that of 1) Loblolly-pine-dominated stands, and 2) conifer-dominated stands in the State of Maryland were performed. Stand 1 exhibits a stocking density (0.140 trees/m^2) that is slightly below average for both Loblolly pine-dominated and conifer-dominated stands in Maryland. Conversely, values of basal area (0.00444 m^2/m^2), volume (0.036 m^3/m^2), and green biomass (45.447 kg/m^2) for this stand appear significantly higher than average. For example, the basal area of Stand 1 is higher than 99.0% of all Loblolly pine-dominated plots (100 plots) and higher than 98.6% (142 plots) of all conifer-dominated plots in the Maryland FIA network. Similarly, green biomass is higher than 99.0% of all Loblolly pine-dominated plots (100 plots) and higher than 99.3% (143 plots) of all conifer-dominated plots. Higher than expected values of basal

area, volume, and biomass might be due to the mature, unmanaged nature of the Loblolly pine/hardwood trees at Stand 1.

Comparisons between the stocking density, basal area, volume, and green biomass of Stand 2 (deciduous) and that of 1) Sweetgum-dominated stands, and 2) nonconifer-dominated (deciduous) stands in the State of Maryland were performed too. Stand 2 exhibits a stocking density (0.1055 trees/m^2) that is slightly below average and basal area (0.00324 m^2/m^2), volume (0.02317 m^3/m^2), and green biomass (30.9 kg/m^2) values that are slightly above average for Sweetgum-dominated stands in Maryland. A similar trend is observed when the broader comparison is made between Stand 2 and all deciduous stands in Maryland. For example, the basal area of Stand 2 (0.00324 m^2/m^2) is higher than that of 77.0% (57 plots) of all Sweetgum-dominated plots and 88.2% (418 plots) of all deciduous plots in the Maryland FIA network. Similarly, the green biomass (30.9 kg/m^2) is higher than 77.0% (57 plots) of all Sweetgum-dominated plots and higher than 75.9% (360 plots) of all deciduous plots.

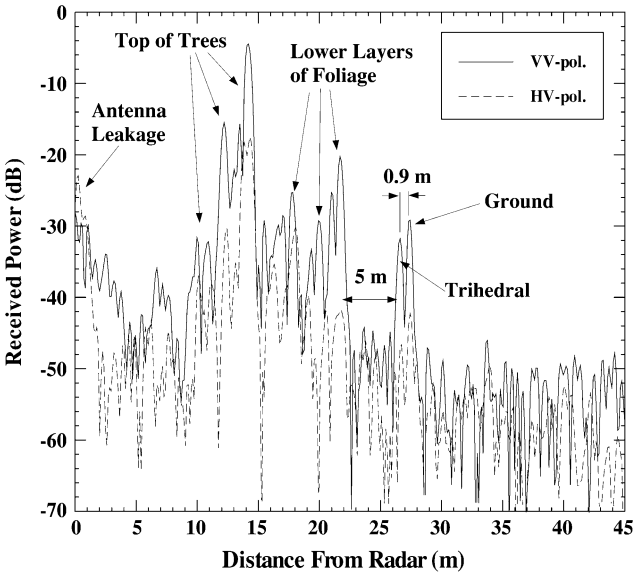

Fig. 6. Example of the measured radar return at 35-GHz at normal incidence that includes the backscatter responses of the canopy, the trihedral, and the ground.

IV. Data Analysis

For any given spot and incidence angle, the measured data, in general, consisted of multiple returns from various scatterers (foliage, trihedral, ground, etc.). Because of the spatial distribution of scatterers, these returns occurred with different time delays that were directly proportional to their distances from the radar. An example of the measured radar return that includes the responses of the canopy, the trihedral, and the ground is shown in Fig. 6. The first step in processing this data was to apply a threshold where only returns with signal-to-noise ratios equal or exceeding 10 dB were retained. Then, heights above ground for each of these returns were determined using the GPS data for the radar system, the time of arrival of that return, and the incidence angle. Once the heights were determined, it was straight forward to isolate the trihedral and ground returns from other nearby returns. An additional constraint was imposed to ensure that the return was indeed from the trihedral. The constraint is that the height of the trihedral return should be about 0.9 m above the ground surface. Once the two returns of interest were identified, (1) through (10) were used to compute the two-way attenuation by the foliage and the reflectivity of the ground surface.

A. Two-Way Foliage Attenuation Data

The sample values for the two-way foliage attenuation factor measured at specific spots (averaged over time) within tree Stand 1 are plotted in Fig. 7(a) for rows 5 and 6. The figure clearly demonstrates the strong spatial variations in foliage attenuation within the tree stand. This in turn is consistent with what was observed physically at the test site. A photograph of the foliage-cover, taken from a point on the ground at Stand 1 showing sky openings, is shown in Fig. 8. It demonstrates the strong spatial variations in foliage density, both vertically and horizontally. Similar to Stand 1, the time-averaged values for the two-way foliage attenuation factor, measured at specific spots within tree Stand 2, were generated and are plotted in Fig. 7(b) for row 31. As discussed before, the measurements in this stand were performed at three different incidence angles. The two-way attenuation for the three sets of incidence angles has been identified in Fig. 7(b) by $-2^\circ, 0^\circ$, and $+2^\circ$. It should be noted that a slight change in the incidence angle on the order of 2 degrees results in substantial fluctuations in the two-way attenuation factor as clearly demonstrated in Fig. 7(b). Hence, for a SAR to successfully image a camouflaged target, its synthetic aperture must subtend an angle much smaller than 2° which is usually the case for the required resolution. However, this angular decorrelation value must be determined. The data collected here indicates that 2° angular change generates completely independent measurements since the radar signal is expected to propagate through different sets of branches and leaves. Hence, the data measured at different incidence angles can be assumed independent and used in generating a histogram of the two-way foliage attenuation factor at Stand 2.

A histogram and the corresponding cumulative distribution function (cdf) of the two-way attenuation data collected at Stand 1 are shown in Fig. 9(a) and (b), respectively. About 26.7% of the data points had attenuation values exceeding 70 dB (the radar backscatter return from the trihedral at 26.7% of the spots fell below the threshold level of the radar and could not be detected) and were not included in the histogram at this stage. However, they were accounted for in the cdf. Similarly, the histogram and cdf of the two-way attenuation collected at Stand 2 are shown in Fig. 10(a) and (b), respectively. In this figure, about 8.64% of the data points had attenuation values exceeding 70 dB and were not included in the histogram. However, they were accounted for in the cdf. It should be noted that the logarithm of the two-way attenuation factor A data (i.e., $10\log_{10} A$) was used in generating the histograms and cdfs of Figs. 9 and 10. To compute the mean, standard deviation, and median of the two-way attenuation factor, the absolute value of A was used. For Stand 1 (mostly coniferous), the mean, standard deviation, and median of the measured two-way attenuation factor, expressed in

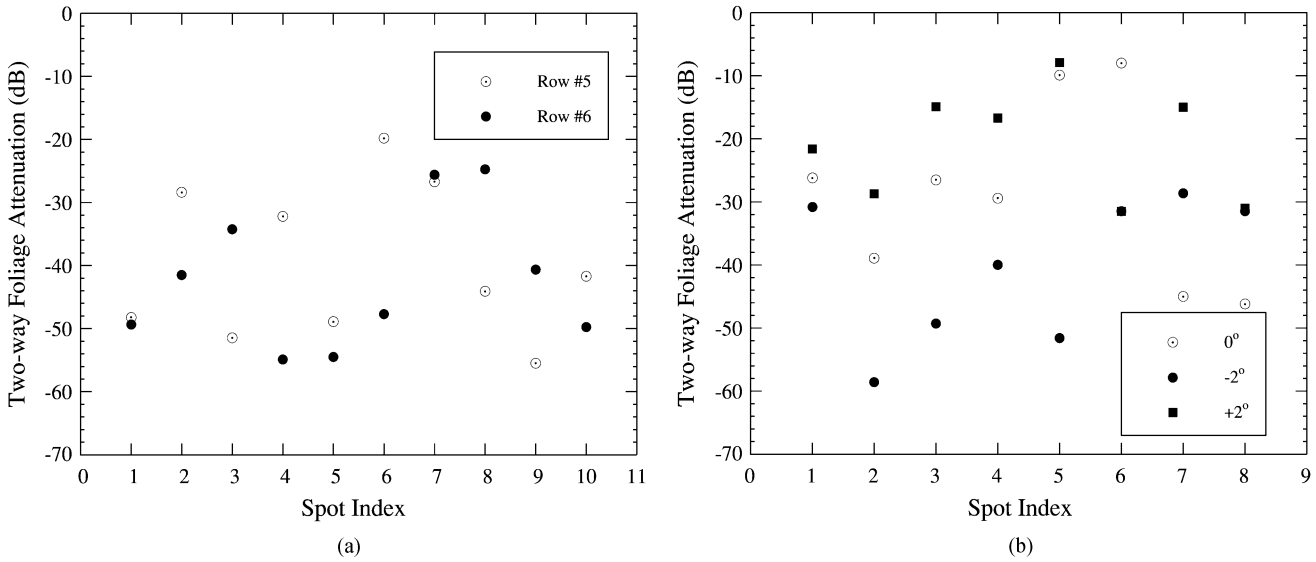

Fig. 7. The mean two-way attenuation factor measured along specific spots in: (a) rows 5 and 6 of Stand 1 (mostly coniferous) and (b) row 31 of Stand 2 (deciduous).

Fig. 8. Photograph of the foliage cover at Stand 1 taken straight up from chest level. The photograph demonstrates the density and strong spatial variations in foliage cover.

decibels, were -25.4, -18.3, and -48.2 dB, respectively. Similarly for Stand 2 (deciduous), the mean, standard deviation, and median of the measured two-way attenuation factor, expressed in decibels, were -15.4, -12.7, and -33.6 dB, respectively. These results indicate that more attenuation is experienced by the signal at Stand 1 when compared to Stand 2. This result is consistent with the ground truth data observations, where the higher stocking density, basal area, and green biomass were measured for Stand 1 when compared to Stand 2. Considering the mean crown thickness, d, for Stands 1 and 2 are 7.3 and 7.4 m, respectively, then the approximate one-way attenuation rates, α (with $\langle A \rangle = e^{(-2\alpha d)}$), measured for Stands 1 and 2 are $\alpha_1 = 0.40$ and $\alpha_2 = 0.24$ Np/m, respectively.

B. Ground Reflectivity Data

Next we present the reflectivity of forest floor extracted from the backscatter measurements of elevated trihedrals embedded in the test sites. An upper bound for the ground reflectivity can be achieved assuming the forest floor is a flat dielectric half-space. A four-component mixing formula can be used for estimating the effective permittivity of a soil medium composed for clay, silt, and water [20]. The effective soil permittivity at 35-GHz of dry and wet (20% volumetric moisture content), respectively, are calculated to be $\varepsilon_d = 2.5$ and $\varepsilon_w = 6 + j3.5$. The corresponding reflection coefficients for these surfaces at nadir incidence are 0.43 and 0.78 which corresponds to the surface reflectivity of -7.3 and -2.2 dB, respectively. Unfortunately, soil samples were not collected from the two sites during the attenuation measurements to determine the moisture content of the soils. Nevertheless, it is expected that between 10% and 20% soil moisture were present in the soil during the measurements. Hence, the value of -2.2 dB can be used as an upper limit for the measured ground reflectivity.

Fig. 11 shows the values of the power (ground) reflectivity derived for various spots in rows 5 and 6 of Stand 1. A strong fluctuation in the power reflectivity is observed from one spot to the next (1 meter apart). In addition, a significant portion of the spots had power reflectivities that were smaller than -20 dB. At many spots within the two stands, no returns were observed from the ground (not shown in Fig. 11). The lack of radar return can be attributed to either strong foliage attenuation or significant ground clutter that destroyed the coherent return from the surface. A close look at the photograph in Fig. 3 reveals the various types of ground litter present in Stand 1 (pine needles, broken branches, fallen tree trunks, etc.). Similar results for the power reflectivity at Stand 2 were observed. In this case though, fewer cases were recorded of power reflectivity. This can be attributed to the fact that in Stand 2, a significant understory foliage structure existed near the ground surface. The result is a more diffuse medium near the surface, hence, a set of weak effective reflection coefficients. Histograms and cdfs of the power reflectivities of the two stands are shown in Figs. 12 and 13. These histograms and cdfs were generated using the logarithm of the power reflectivity data. To compute the mean, standard deviation and median of the power reflectivity, the absolute values were used. For Stand 1, the mean, standard deviation,

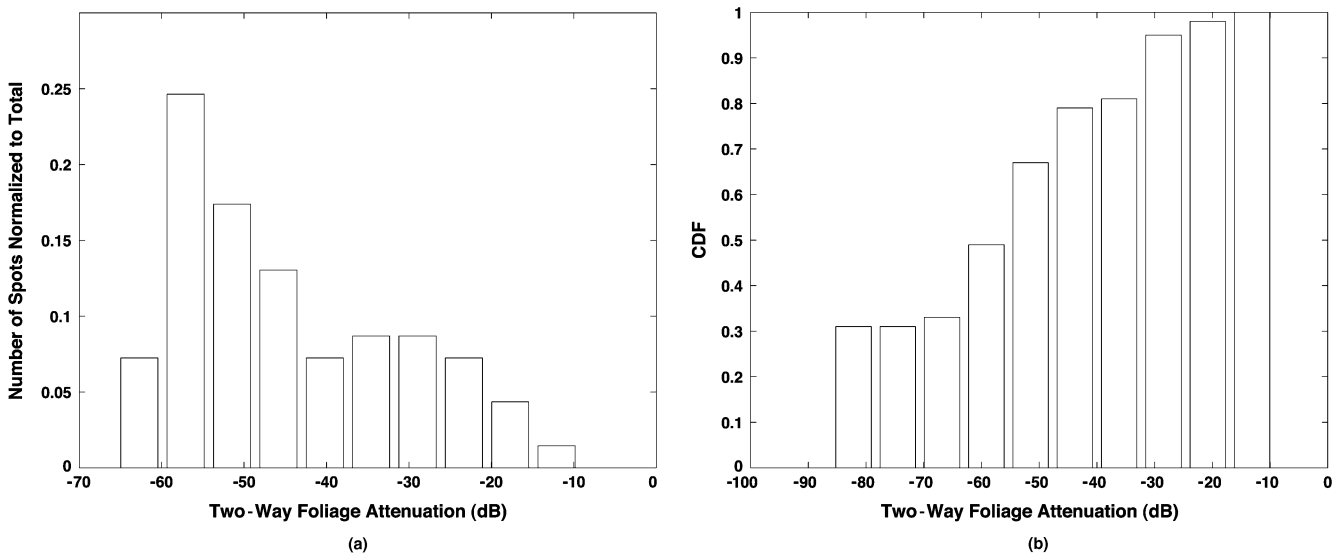

Fig. 9. Histogram (a) and cdf (b) depicting the distribution of the two-way foliage attenuation (in dB) at Stand 1.

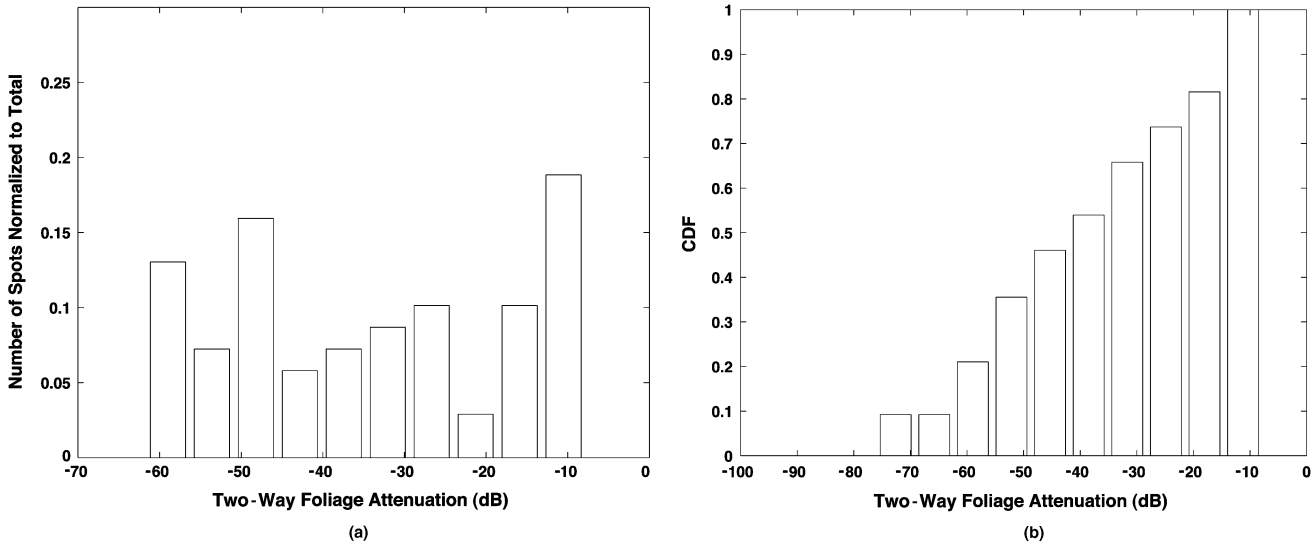

Fig. 10. Histogram (a) and cdf (b) depicting the distribution of the two-way foliage attenuation (in dB) at Stand 2.

and median of the power reflectivity, expressed in decibels, were -14.2, -11.0, and -21.1 dB, respectively. Similarly for Stand 2, the mean, standard deviation, and median of the power reflectivity, expressed in decibels, were -16.0, -14.3, and -22.2 dB, respectively.

The weak power reflectivities reported in Figs. 11–13 might be somewhat misleading in a sense that one could conclude that detection of the return from ground in the presence of foliage cover requires significant transmitter power. However, it should noted that the radar return from the ground surface at nadir incidence is governed primarily by (5) derived from the *Friis* formula as opposed to the radar equation. That is, the range dependence of the received power is proportional to $1/R^2$ as opposed to $1/R^4$ which is considered in the calculation of the signal to noise ratio for a radar system. For example, consider a real aperture, nadir-looking 35 GHz ($\lambda = 8.571$ mm) radar operating at an altitude of 500 m (1667 ft) above ground and transmitting 1 watt in total power. In addition, let the radar's bandwidth, B, aperture size, l, and foot-print on ground be

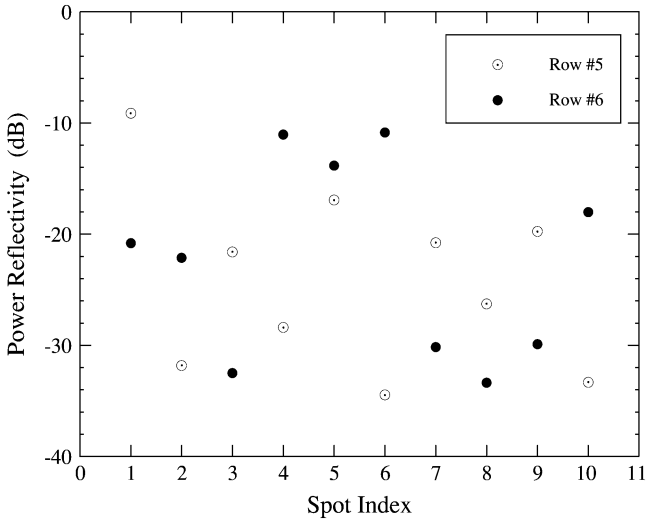

Fig. 11. Measured power reflectivity at specific spots in rows 5 and 6 at Stand 1 (mostly coniferous foliage).

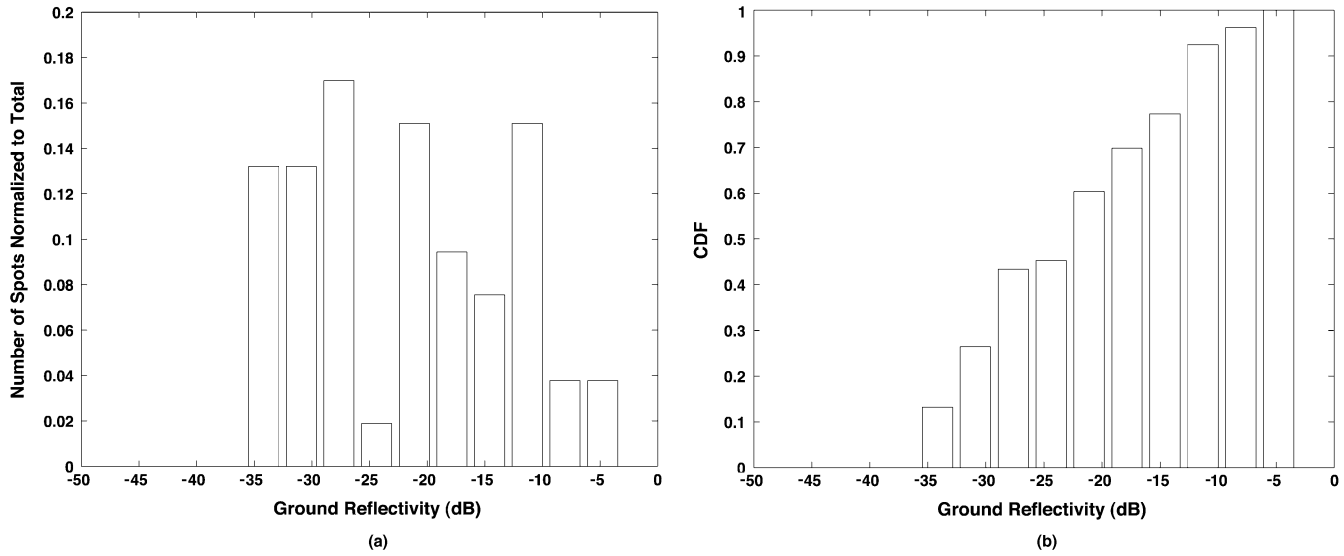

Fig. 12. Histogram (a) and cdf (b) of ground reflectivity (in decibels) of Stand 1.

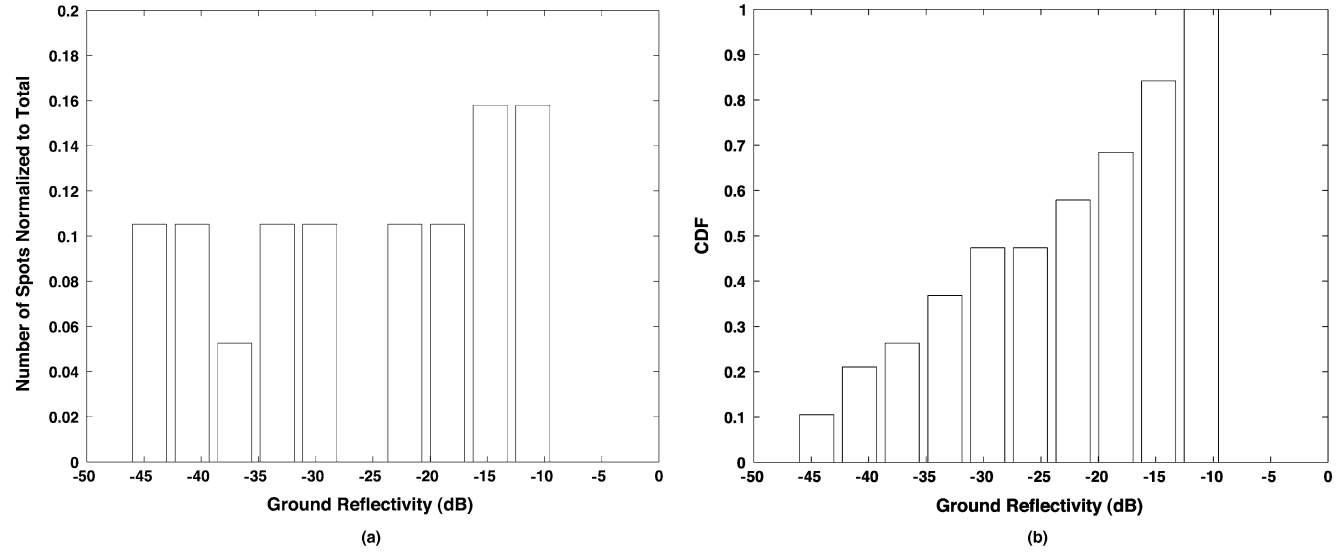

Fig. 13. Histogram (a) and cdf (b) of ground reflectivity (in decibels) at Stand 2.

500 MHz, 2.0 m, and 2.14 m, respectively. Using approximate formulas for the antenna gain, G, and beamwidth, β, namely, $\beta = \lambda/l$ and $G = (2\pi)/\beta^2$, the received power from the forest ground can be computed using (5) for a given two-way foliage attenuation factor and ground reflectivity. The received power from ground is plotted in Fig. 14 as a function of ground reflectivity. Four different two-way foliage attenuation factors were considered. With the detection threshold set to 10 dB above the system thermal noise level, it is apparent that except for cases where both the two-way foliage attenuation factor is high and the ground reflectivity is weak, the ground return can be detected easily. In these calculations, the noise power is obtained from kT_oB, where k is Boltzman constant and T_o is the ambient temperature and assuming that the forest emissivity is unity. The expected received returns from the ground surface when this system is operated over Stands 1 and 2 are shown in Fig. 14 too.

V. Conclusion

The two-way foliage attenuation and ground reflectivity of two different tree stands, one mostly coniferous and the other deciduous, were measured using a nadir-looking, high-resolution, 35-GHz radar positioned above the tree canopy. In addition to radar measurements, the physical characteristics of vegetation-cover at the two stands were determined and compared to regional stands. The radar data demonstrated a strong spatial and angular fluctuations of the two-way foliage attenuation factor. Despite the high basal area, volume, and biomass and low percentage open sky of both stands when compared to

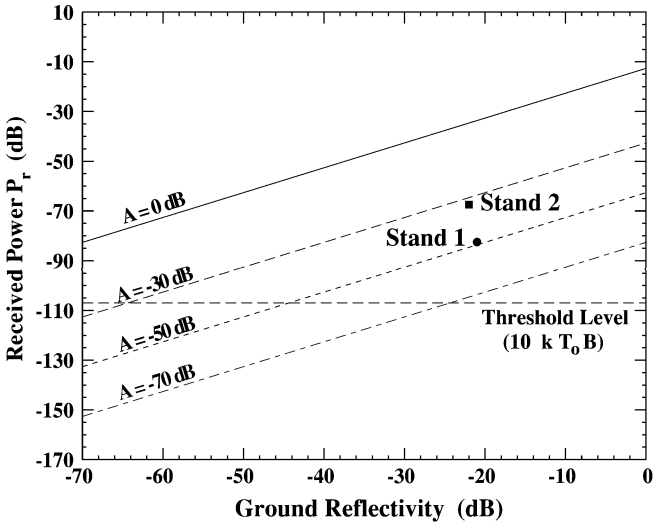

Fig. 14. Received power of a 2.0-m, real aperture, nadir-looking radar operating at 35 GHz computed as a function of the ground reflectivity. Four different two-way foliage attenuation factors were considered. The radar is at an altitude of 500 m and its foot print on the ground is 2 m in diameter. The expected received returns from the ground surface when this system is operated over Stands 1 and 2 were demonstrated too.

similar regional stands, the mean (median) two-way foliage attenuation in Stand 1 and Stand 2 were -25.4 (-48.2 dB) and -15.4 dB (-33.6 dB), respectively. Only 26.7% and 8.64% of the measured spots under the canopy in stands 1 and 2, respectively, had two-way foliage attenuations exceeding 70 dB. It was also observed that the ground reflectivity is tempered significantly by the amount and character of the ground litter. The presence of a dense understory/ground-cover is expected to reduce the ground reflectivity significantly. The mean (median) power reflectivity of the forest floors at Stands 1 and 2 are -14.2 dB (-21.1 dB) and -16.0 dB(-22.2 dB), respectively. These results demonstrate the potential for using MMW nadir-looking radars for the detection of targets underneath foliage.

ACKNOWLEDGMENT

The authors would like to thank Dr. L. Pierce for his role in classifying photos of the tree stands, and Dr. R. D. De Roo and P. Tchou of The University of Michigan, and D. Robertson, C. Deluca, S. Tenney, D. Testerman, and R. Tan of ARL for their assistance during the measurements.

REFERENCES

[1] B. Ferrell, "Ultrawideband foliage penetration measurements," in *Proc. IEEE Nation Radar Conf.*, Mar. 29–31, 1994, pp. 80–84.

[2] L. Happ, K. A. Kappra, M. A. Ressler, J. P. Sichina, K. Sturgess, and F. Le, "Low-frequency ultra-wideband synthetic aperture radar 1995 BoomSAR tests," in *Proc. IEEE National Radar Conf.*, Ann Arbor, MI, May 13–16, 1996, pp. 54–59.

[3] B. T. Binder, M. F. Toups, S. Ayasli, and E. M. Adams, "SAR foliage penetration phenomenology of tropical rain forest and northern U.S. forest," in *Proc. IEEE International Radar Conf.*, May 8–11, 1995, pp. 158–163.

[4] S. Ayasli and L. Bessette, "UHF & VHF SAR phenomenology," presented at the Proc. PIERS, Workshop on Advances in Radar Methods, Baveno, Italy, July 20–22, 1998.

[5] L. Carin, N. Geng, M. McClure, J. Sichina, and L. Nguyen, "Ultra-wide-band synthetic-aperture radar for mine-field detection," *IEEE Antennas Propagat. Mag.*, vol. 41, pp. 18–33, Feb. 1999.

[6] I. S. Koh and K. Sarabandi, "Polarimetric channel characterization of foliage for performance assessment of receivers under tree canopies," *IEEE Trans. Antennas Propagat.*, vol. 50, no. 5, pp. 713–726, May 2002.

[7] C. C. Borel and R. E. McIntosh, "Millimeter wave backscatter from deciduous trees," *IEEE Trans. Antennas Propagat.*, vol. 38, pp. 1391–1398, Sept. 1990.

[8] R. M. Narayanan, C. C. Borel, and R. E. McIntosh, "Radar backscatter characteristics of trees at 215 GHz," *IEEE Trans. Geosci. Remote Sensing*, vol. 26, pp. 217–228, May 1988.

[9] J. B. Mead, P. M. Langlois, P. S. Chang, and R. E. McIntosh, "Polarimetric scattering from natural surfaces at 225 GHz," *IEEE Trans. Antennas Propagat.*, vol. 39, pp. 1401–1411, Sept. 1991.

[10] N. C. Currie, F. B. Dyer, and E. E. Martin, "Millimeter foliage penetration measurements," presented at the Proc. Int. IEEE Antennas and Propagat. Soc. Symp. Digest, Amherst, MA, 1976.

[11] E. J. Violette, R. H. Espeland, and F. Schwering, "Vegetation loss measurements at 9.6, 28.8, and 57.6 GHz through a pecan orchard," in *CECOM-83-2*. Fort Monmouth, NJ, Mar. 1983.

[12] F. K. Schwering, E. J. Violette, and R. H. Espeland, "Millimeter-wave propagation in vegetation: Experiments and theory," *IEEE Trans. Geosci. Remote Sensing*, vol. 26, pp. 355–367, May 1988.

[13] F. T. Ulaby, T. E. Van Deventer, J. R. East, T. F. Haddock, and M. E. Coluzzi, "Millimeter-wave bistatic scattering from ground and vegetation targets," *IEEE Trans. Geosci. Remote Sensing*, vol. 26, pp. 229–243, May 1988.

[14] A. Nashashibi, F. T. Ulaby, P. Frantzis, and R. D. De Roo, "Measurements of the propagation parameters of tree canopies at MMW frequencies," *IEEE Trans. Geosci. Remote Sensing*, vol. 40, pp. 298–304, Feb. 2002.

[15] A. Nashashibi, F. T. Ulaby, and K. Sarabandi, "Measurement and modeling the millimeter-wave backscatter response of soil surfaces," *IEEE Trans. Geosci. Remote Sensing*, vol. 34, pp. 561–572, Mar. 1996.

[16] F. T. Ulaby, A. Nashashibi, A. El-Rouby, E. Li, R. DeRoo, K. Sarabandi, R. Wellman, and B. Wallace, "95-GHz scattering by terrain at near grazing incidence," *IEEE Trans. Antennas Propagat.*, vol. 46, pp. 3–13, Jan. 1998.

[17] A. Nashashibi, K. Sarabandi, P. Frantzis, R. D. De Roo, and F. T. Ulaby, "An ultra-fast wideband MMW polarimetric radar for remote sensing applications," IEEE Trans. Geosci. Remote Sensing, vol. 40, pp. 1777–1786, Aug. 2002, submitted for publication.

[18] T. C. Chiu and K. Sarabandi, "Electromagnetic scattering interaction between a dielectric cylinder and a slightly rough surface," *IEEE Trans. Antennas Propagat.*, vol. 47, May 1999.

[19] F. T. Ulaby and C. Elachi, *Radar Polarimetry for Geoscience Applications*. Norwood, MA: Artech House, 1990, p. 62.

[20] F. T. Ulaby, R. K. Moore, and A. K. Fung, *Microwave Remote Sensing*. Norwood, MA: Artech House, 1986, vol. III.

Adib Y. Nashashibi (S'82–M'95–SM'01) received the B.Sc. and M.Sc. degrees in electrical engineering from Kuwait University, Kuwait, in 1985 and 1988, respectively, and the Ph.D. degree in electrical engineering from The University of Michigan, Ann Arbor, in 1995.

He is presently an Associate Research Scientist at the Radiation Laboratory at The University of Michigan. His research interests include microwave and millimeter-wave remote sensing, polarimetric radar calibration and measurement techniques, bistatic radar phenomenology, electromagnetic wave propagation, and scattering in random media.

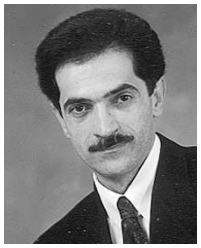

Kamal Sarabandi (S'87–M'90–SM'92–F'00) received the B.S. degree in electrical engineering from Sharif University of Technology, Tehran, Iran, in 1980, and the M.S. degree in electrical engineering and mathematics and the Ph.D. degree in electrical engineering from The University of Michigan, Ann Arbor, in 1986 and 1989, respectively.

He is Director of the Radiation Laboratory and a Professor in the Department of Electrical Engineering and Computer Science, The University of Michigan. He has 20 years of experience with wave propagation in random media, communication channel modeling, microwave sensors, and radar systems and is leading a large research group. He has served as the Principal Investigator on many projects sponsored by NASA, JPL, ARO, ONR, ARL, NSF, DARPA, and numerous industries. He has published many book chapters and more than 105 papers in refereed journals on electromagnetic scattering, random media modeling, wave propagation, antennas, microwave measurement techniques, radar calibration, inverse scattering problems, and microwave sensors. He has had more than 220 papers and invited presentations in national and international conferences and symposia on similar subjects. Over the past ten years he has graduated 20 Ph.D. students. His research interests include microwave and millimeter-wave radar remote sensing, electromagnetic wave propagation, and antenna miniaturization.

Dr. Sarabandi is a Member of URSI Commission F and of The Electromagnetic Academy. He received the Henry Russel Award from the Regent of The University of Michigan (the highest honor The University of Michigan bestows on a faculty member at the assistant or associate level). In 1999, he received a GAAC Distinguished Lecturer Award from the German Federal Ministry for Education, Science, and Technology. He also received a 1996 Teaching Excellence Award from the Department of Electrical Engineering and Computer Science, and the 2003 to 2004 College of Engineering Research Excellence Award, The University of Michigan. He is a Vice President of the IEEE Geoscience and Remote Sensing Society (GRSS), a past Chairman of the Awards Committee of the IEEE GRSS from 1998 to 2002, and a Member of the IEEE Technical Activities Board Awards Committee from 2000 to 2002. He is Associate Editor of the IEEE TRANSACTIONS ON ANTENNAS AND PROPAGATION (AP) and the IEEE SENSORS JOURNAL. He is listed in *American Men & Women of Science, Who's Who in America,* and *Who's Who in Electromagnetics.*

Shadi Oveisgharan was born in Isfahan, Iran, in 1977. She received the B.Sc. from Sharif University of Technology, Tehran, in 1999 and the M.S. degree from The University of Michigan, Ann Arbor, in 2002, both in electrical engineering. She is currently working toward the Ph.D. degree in the STAR LAB at Stanford University, Stanford, CT.

From 2000 to 2002, she worked as a Graduate Research Assistant with the Radiation Laboratory, University of Michigan. Her current research interests include electromagnetic scattering theory and radar remote sensing.

M. Craig Dobson (SM'91) received the B.A. degree in Geology and Anthropology from the University of Pennsylvania, Philadelphia, in 1973 and the M.S. degree in Geography from the University of Kansas, Lawrence, in 1981.

He was previously with the Center for Research, University of Kansas. He is on leave from his position as Research Scientist with The University of Michigan, Ann Arbor, where he has been a member of the Research Faculty at the Radiation Lab since 1984. He is currently a Program Scientist with the Office of Earth Science at National Aeronautics and Space Administration (NASA) Headquarters, Washington, DC.

His interests include basic and applied research in the field of microwave remote sensing. His prior work includes measurement and modeling of the fundamental microwave dielectric properties of natural terrestrial media (soil, vegetation, and snow) and understanding the microwave emission and radar backscattering from terrain. Basic research is conducted in the laboratory and field experiments using truck-mounted, airborne, and orbital instrumentation have lead to applied research in the areas of remote sensing of near-surface soil moisture, land-cover classification, and the retrieval of biophysical estimates of vegetation attributes such as height, basal area, above-ground biomass, timber volume, and carbon storage. This work has been extended to simulation of the expected performance of the next generation of orbital SAR systems now being designed and constructed by Japan, Canada, Europe, and the United States. He is currently engaged in large-scale assessment of tropical forests using archival SAR data and joint projects with the U.S. Forest Service and timber companies to evaluate the use of SAR for forest assessment and management. Much of this research has been done in close collaboration with ecologists, soil scientists, foresters, and hydrologists in an interdisciplinary setting.

Wayne S. Walker received the B.S. degree in resource ecology and management and the M.S. degree in forest/terrestrial ecology from The University of Michigan, Ann Arbor, in 1994 and 1999, respectively, where he is currently working toward the Ph.D. degree in remote sensing from the School of Natural Resources and Environment, The University of Michigan.

He is currently a Graduate Student Research Assistant in the Radiation Laboratory, Electrical Engineering and Computer Science Department, The University of Michigan. His current research interests include the quantification and description of forest ecosystem structure, specifically evaluating the potential of multisensor fusion techniques for use in estimating structural and biomass characteristics of forests.

E. Burke (M'92–SM'00) was born in 1951. He received the B.E. degree from Stevens Institute of Technology, Hoboken, NJ, in 1973 and the M.S.E.E. degree from the University of Maryland, College Park, in 1976.

He joined the U.S. Army Harry Diamond Laboratories in 1972 and worked on radar fuzing until the formation of the Army Research Labs in 1992. Since then, he has been the Chief of the RF and Electonics Division and is currently Chief of the Millimeter Wave Branch in the Sensors and Electron Devices Directorate of the Army Research Lab. His research interests include MMW phenomenology and architectures for military systems.